NeuroImage: Clinical 36 (2022) 103188

Contents lists available at ScienceDirect

NeuroImage: Clinical

journal homepage: www.elsevier.com/locate/ynicl

A direct comparison of voice pitch processing in acoustic and electric hearing

Kurt Steinmetzger [a,*], Bastian Meinhardt [a], Mark Praetorius [b], Martin Andermann [a], André Rupp [a]

[a] Section of Biomagnetism, Department of Neurology, Heidelberg University Hospital, Im Neuenheimer Feld 400, 69120 Heidelberg, Germany
[b] Section of Otology and Neurootology, ENT Clinic, Heidelberg University Hospital, Im Neuenheimer Feld 400, 69120 Heidelberg, Germany

ARTICLE INFO

Keywords:
Cochlear implants
EEG source reconstructions
fNIRS
Prosody
Single-sided deafness
Speech

ABSTRACT

In single-sided deafness patients fitted with a cochlear implant (CI) in the affected ear and preserved normal hearing in the other ear, acoustic and electric hearing can be directly compared without the need for an external control group. Although poor pitch perception is a crucial limitation when listening through CIs, it remains unclear how exactly the cortical processing of pitch information differs between acoustic and electric hearing. Hence, we separately presented both ears of 20 of these patients with vowel sequences in which the pitch contours were either repetitive or variable, while simultaneously recording functional near-infrared spectroscopy (fNIRS) and EEG data. Overall, the results showed smaller and delayed auditory cortex activity in electric hearing, particularly for the P2 event-related potential component, which appears to reflect the processing of voice pitch information. Both the fNIRS data and EEG source reconstructions furthermore showed that vowel sequences with variable pitch contours evoked additional activity in posterior right auditory cortex in electric but not acoustic hearing. This surprising discrepancy demonstrates, firstly, that the acoustic detail transmitted by CIs is sufficient to distinguish between speech sounds that only vary regarding their pitch information. Secondly, the absence of a condition difference when stimulating the normal-hearing ears suggests a saturation of cortical activity levels following unilateral deafness. Taken together, these results provide strong evidence in favour of using CIs in this patient group.

1. Introduction

A major challenge when studying functional brain activity in clinical populations is that the control groups required to evaluate the results can only be matched for a limited set of parameters. Here, we present data from a group of adults with single-sided deafness (SSD), all of which were fitted with cochlear implants (CIs) in the deafened ear but had preserved normal acoustic hearing in the other ear, resulting in the rare scenario that each participant acted as their own control subject. Separately stimulating both ears allowed for a direct comparison of acoustic hearing and CI-based electric hearing.

CIs have proven very successful in restoring hearing after profound sensorineural hearing loss (Macherey and Carlyon, 2014; Wilson and Dorman, 2008). Yet, the electrical components of the devices have hindered the study of brain activity in CI users, particularly the use of functional MRI and MEG. EEG data obtained from CI users, on the other hand, are severely affected by electrical artefacts, and a substantial part of the literature has focussed on ways to remove them (Friesen and Picton, 2010; Gilley et al., 2006; Viola et al., 2012; Viola et al., 2011). Therefore, PET has been applied extensively in CI research (Anderson et al., 2017a; Strelnikov et al., 2015), despite its inconvenience. More recently, however, functional near-infrared spectroscopy (fNIRS) has been identified as an ideal CI-compatible imaging method (Anderson et al., 2017a; Pinti et al., 2018).

The majority of PET studies with CI users focussed on how the processing of speech is affected by deafness-induced plasticity effects in auditory and visual cortex and how these relate to CI-based speech intelligibility (Coez et al., 2008; Giraud et al., 2001a; Giraud et al.,

Abbreviations: CI, Cochlear implant; EEG, Electroencephalography; ERPs, Event-related potentials; fNIRS, Functional near-infrared spectroscopy; GLM, General linear model; HbO, Oxygenated haemoglobin; HbR, De-oxygenated haemoglobin; HRF, Haemodynamic response function; NH, Normal-hearing; MEG, Magneto-encephalography; PET, Positron emission tomography; ROI, Region of interest; SACFs, Summary autocorrelation functions; SCI, Scalp coupling index; SP, Sustained potential; SPM, Statistical parametric mapping; SSD, Single-sided deafness; STC, Superior temporal cortex.

* Corresponding author.
E-mail address: kurt.steinmetzger@uni-heidelberg.de (K. Steinmetzger).

https://doi.org/10.1016/j.nicl.2022.103188
Received 2 June 2022; Received in revised form 24 August 2022; Accepted 6 September 2022
Available online 10 September 2022

2001b; Giraud et al., 2000; Green et al., 2005; Mortensen et al., 2006; Rouger et al., 2012; Strelnikov et al., 2013). Similarly, most fNIRS studies with CI users to date were concerned with cortical activity elicited by visually or auditorily presented speech (Anderson et al., 2017b; Bisconti et al., 2016; Chen et al., 2016; Mushtaq et al., 2020; Olds et al., 2016; Sevy et al., 2010; van de Rijt et al., 2016; Zhou et al., 2018). Although a few PET (Giraud et al., 2001a; Giraud et al., 2001b; Giraud et al., 2000; Mortensen et al., 2006) and fNIRS studies (Chen et al., 2017a; Chen et al., 2017b; Mushtaq et al., 2020; Olds et al., 2016) also used vowels or non-speech stimuli, systematic comparisons of basic auditory perception processes in CI users and normal-hearing (NH) controls are lacking. This is particularly striking with regard to pitch perception, which is very limited when listening through a CI and a crucial factor underlying the difficulties CI users encounter when listening to speech and music, especially in background noise (Green et al., 2004; Oxenham, 2008; Steinmetzger and Rosen, 2018). The only pitch cues available to CI users are the periodic fluctuations of the temporal envelope of the acoustic input and hence their ability to identify the voice pitch contours that constitute a major part of prosody is strongly reduced (Chatterjee and Peng, 2008; Everhardt et al., 2020).

Here, the participants were presented with continuous sequences of natural vowels in which the pitch contours were either the same throughout or varied between the individual vowels, while controlling for spectro-temporal differences between the two conditions. This subtle but linguistically relevant acoustic contrast allowed us to compare the processing of voice pitch changes in acoustic and electric hearing. Concurrent fNIRS and EEG data were obtained while stimulating each ear separately to study the evoked haemodynamic and electrophysiological activity. Furthermore, source reconstructions of the resulting event-related potentials (ERPs) were computed to investigate the interrelation of both types of cortical activity in detail. To date, there is only one concurrent fNIRS-EEG study with CI users (Chen et al., 2017b), which reported lower adaptation rates to visual and auditory stimuli compared to NH controls, but this study neither examined the distribution of cortical activity in detail nor did it include source-level ERP analyses.

Previously, we tested young NH listeners with the same paradigm and methodology to obtain results the present data can be compared with and to assess the congruence of the two imaging methods (Steinmetzger et al., 2022). Both the fNIRS topographies and the ERP source reconstructions showed strongly right-lateralised activity in superior temporal areas for both types of vowel sequences. Sequences with variable prosodic contours, however, elicited additional cortical activity along the right superior temporal cortex (STC), particularly its anterior portion. The source-level ERPs revealed that this additional activity was driven by increased P2 and sustained potential amplitudes. These results are in line with the notion that pitch changes are primarily processed in superior temporal areas located anterior to right primary auditory cortex (Johnsrude et al., 2000; Patterson et al., 2002; Zatorre and Belin, 2001).

It is unclear, however, if these areas are also involved in the processing of voice pitch changes in CI-based hearing and whether the same degree of hemispheric specialisation applies. Due to the limited spectral resolution of the devices, it has been suggested that pitch changes may be perceived as changes in brightness or timbre rather than actual variations of pitch (Oxenham, 2008). Accordingly, the additional activity in the variable prosody condition should be confined to central and posterior portions of right STC, where slow spectro-temporal modulations elicit the strongest responses in normal hearing (Boemio et al., 2005; Poeppel, 2003). Previous EEG studies with CI users have shown a reduced mismatch negativity to pitch changes relative to normal hearing (Kelly et al., 2005; Sandmann et al., 2009; Sandmann et al., 2010), a smaller N1 evoked by pitch onsets (Wagner et al., 2017), and that auditory ERPs hardly differed in response to tones with different degrees of frequency modulation (Sandmann et al., 2015). Yet, the distribution of cortical activity in CI-based pitch processing cannot be inferred from these results.

More generally, both diminished haemodynamic cortical activity in auditory areas (Coez et al., 2008; Giraud et al., 2000) as well as smaller and delayed auditory ERPs (Agrawal et al., 2013; Kelly et al., 2005; Sandmann et al., 2009; Sandmann et al., 2015; Viola et al., 2011; Wagner et al., 2017) have been observed in CI users relative to NH controls using different types of auditory stimuli. These effects were shown to increase with the duration of deafness before implantation (Green et al., 2005; Kelly et al., 2005; Sandmann et al., 2010; Viola et al., 2011) and possible explanations for them include the lower number of activated neurons as well as a reduction of synchronised neural activity caused by the limited sensory input provided by CIs (Agrawal et al., 2013; Sandmann et al., 2009). However, these differences between acoustic and electric hearing have never been shown in the same group of subjects. Similar effects in the current sample of unilateral CI users with preserved contralateral acoustic hearing, particularly regarding the delayed ERPs, would thus imply temporally disparate neural responses despite several years of experience with bimodal hearing.

2. Material and methods

2.1. Participants

Twenty participants with SSD, i.e., unilateral CI users with preserved normal acoustic hearing in the contralateral ear, took part in this experiment. All subjects were post-lingually deafened German native speakers. According to the current WHO (2021), three subjects had a moderate hearing loss in the contralateral ear (35–50 dB average hearing level from 0.5 to 4 kHz; subjects 5, 17 & 20). For all other subjects, the audiometric thresholds only showed some age-typical high-frequency hearing loss at the time of implantation (Fig. 1). None of the participants wore a hearing aid in the contralateral ear or were receiving clinical treatment for hearing loss in the non-implanted ear when the experiment was conducted, indicating that their audiometric thresholds have not deteriorated significantly. Detailed information regarding the participants is provided in Table 1. The words correct scores for the CI ears were determined with the Freiburg monosyllabic speech intelligibility test at a presentation level of 65 dB SPL (Hahlbrock, 1953). Written consent was obtained prior to the experiment. The study was approved by the local research ethics committee (Medical Faculty, University of Heidelberg) and was conducted in accordance with the Declaration of Helsinki.

2.2. Stimuli

The materials used in this study were identical to those employed in a previous fNIRS-EEG experiment with young NH listeners (Steinmetzger et al., 2022), where the stimulus construction is described in more

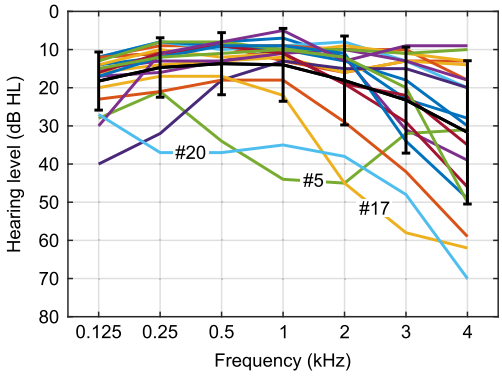

Fig. 1. Audiograms of the non-implanted ears. The coloured lines show the thresholds of the individual subjects, the thick black line indicates the group mean values with standard deviations shown as error bars. Subjects with moderate hearing loss are indicated by black numbers.

Table 1
Subject information[a].

Subject	Age	Sex	CI ear	Duration SSD (~years)	Duration CI use (years,months)	Aetiology of deafness	CI & processor type / strategy	Words correct CI ear (%)
1	58	m	l	23	5.5	Intracochlear schwannoma	FLEX28 & OPUS2 / FS4-p	60
2	61	f	r	6	5.6	Acoustic neuroma	FLEX28 & OPUS2 / FS4	65
3	59	f	l	1	2.2	Sudden hearing loss	HiRes90K & Naida Q90 / HiRes Optima-S	45
4	66	f	r	26	2.6	Sudden hearing loss	FLEX28 & RONDO / FS4-p	65
5	66	f	l	22	5.6	Sudden hearing loss	FLEX28 & OPUS2 / FS4	10
6	67	f	l	1	5.2	Sudden hearing loss	CONCERTO medium & OPUS2 / FS4-p	45
7	66	m	r	1	6.1	Sudden hearing loss	CI422 & CP810 / ACE	70
8	55	f	r	39	6.1	Mumps	FLEX28 & OPUS2 / FS4	55
9	50	f	l	1	5.9	Sudden hearing loss	FLEX28 & OPUS2 / FS4-p	45
10	44	f	r	2	4.4	Otosclerosis	CI522 & CP910 / ACE	55
11	67	f	r	1	6.7	Sudden hearing loss	CI422 & CP810 / ACE	35
12	42	f	r	1	5.3	Sudden hearing loss	HiRes90K & Naida Q90 / HiRes Optima-S	80
13	63	f	l	3	3.7	Sudden hearing loss	FLEX28 & RONDO / FS4-p	55
14	77	f	r	13	2.10	Ménière's / Sudden hearing loss	FLEX28 & SONNET / FS4	30
15	60	m	r	1	3.7	Sudden hearing loss	FLEX28 & RONDO / FS4-p	35
16	78	f	r	1	5.0	Sudden hearing loss	FLEX28 & SONNET / FS4	35
17	70	m	r	1	2.1	Sudden hearing loss	HiRes Ultra & Naida Q90 / HiRes Optima-S	70
18	26	f	r	1	3.4	Meningitis / Temporal bone fracture	FLEX28 & SONNET / FS4	80
19	66	m	r	30	1.4	Sudden hearing loss	FLEX28 & RONDO2 / FS4-p	55
20	58	m	l	20	4.1	Unknown	HiRes90K & Naida Q70 / HiRes Optima-S	90
	Ø = 60 (12)	**f = 14**	**r = 13**	**Ø = 10 (12)**	**Ø = 4.3 (1.7)**	**Sudden hearing loss = 14**	**MED-EL = 13**	**Ø = 54 (19.6)**

[a] Group means (standard deviations) and overall counts, respectively, are provided in the bottom row.

detail. The stimulus materials were recordings of the German vowels /a/ , /e/, /i/, /o/, and /u/ spoken by an adult male German talker. Each vowel was limited to a length of 800 ms using a 50-ms Hann-windowed offset ramp, and re-synthesised with a range of prosodic contours (flat, rising straight, falling straight, rising curved, and falling curved) and two mean fundamental frequencies (*F*0s; 80 Hz and 120 Hz) with the STRAIGHT vocoder software (Kawahara and Irino, 2005). For the non-flat contours, the *F*0 increased or decreased by a perfect fifth relative to the mean *F*0 of the contour. To limit the influence of high-frequency hearing loss in the non-implanted ears, the stimuli were low-pass filtered at 3.5 kHz and then normalised to a common root-mean-square level. Waveforms and narrow-band spectrograms of an example vowel synthesised with the five different prosodic contours are shown in Fig. 2A. To visualise the contours, the lower row of the plot shows spectrographic representations of summary autocorrelation functions (SACFs), as described in Steinmetzger et al. (2022), where the time lag of the first peak represents the pitch contour.

2.3. Experimental design and procedure

The experimental design was identical to that described in Steinmetzger et al. (2022), except that each subject completed the experiment twice, once for the NH ear and once for the CI ear. The order of the two sessions was counterbalanced and each subject went through the whole testing procedure on the same day.

The individual vowels were presented in continuous blocks (20 vowels/16 s) followed by pauses (16–20 s), as shown in Fig. 2B. The experiment consisted of two conditions: In the FIXED PROSODY condition, all vowels within a block had the same prosodic contour (*flat*, *rising straight*, *falling straight*, *rising curved*, or *falling curved*). In the VARIABLE PROSODY condition, the contours varied between the vowels within each block (*rising*, *falling*, *straight*, *curved*, or a *mixture of all five contour types*). The five different contour types were intended to represent a set of typical, easily distinguishable prosodic contours found across languages. The range of prosodic contours, vowels, and F0s was primarily included to ensure the generalisability of the results and to make the experiment less monotonous. Every participant was presented with 50 blocks per condition, in random order. Each session of the experiment thus consisted of 100 stimulus blocks, amounting to a duration of about 57 mins. As the EEG data were analysed relative to the onset of the individual vowels in each block, this design resulted in 2000 trials per session.

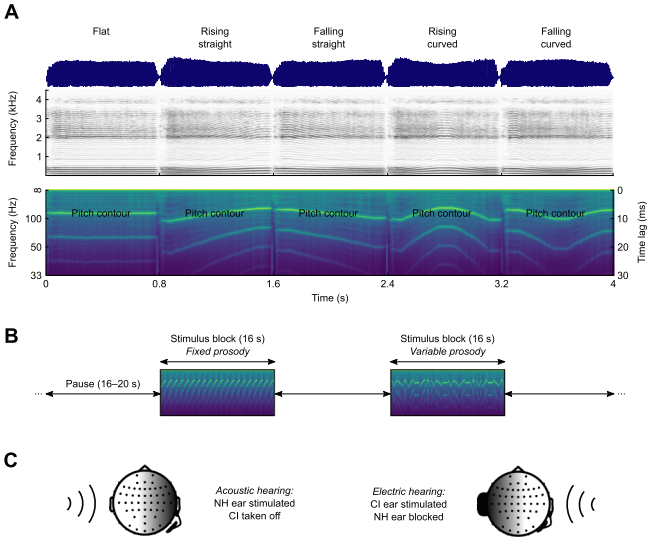

Fig. 2. Example stimuli and experimental design. A) Waveforms, narrow-band spectrograms, and summary autocorrelation function spectrograms of the example vowel /e/ (*F*0 = 120 Hz) synthesised with five different prosodic contours. B) The individual vowels were concatenated into blocks of 20 vowels, alternating with pauses of similar duration. C) Schematic representation of the two test sessions, in which either only the NH ear or only the CI ear received auditory input.

Both ears were tested using free-field acoustic stimulation, for which the stimuli were converted with 24-bit resolution at a sampling rate of 48 kHz using an ADI-8 DS sound card (RME, Haimhausen, Germany) and presented via an Adam A7x speaker (Adam Audio, Berlin, Germany). The speaker was placed directly in front of the listener, ~1.5 m away and at ear level. The presentation level was set to 70 dB SPL using a sound level meter (Brüel & Kjær, type 2235; Nærum, Denmark) placed at the position of the subject's head. When testing the CI ear, the normal ear was blocked with a combination of earplug (3M Series 1100; Maplewood, MN, USA; ~37 dB attenuation) and over-ear hearing protection (3M Peltor Optime III H540A; ~35 dB attenuation). To test the NH ear, the external CI processor was taken off (Fig. 2C). The experiment took place in a sound-attenuating and electrically shielded room, with the participant sitting in a comfortable reclining chair during data acquisition. To minimise ambient light from interfering with the recordings, the participants wore an overcap and the room light was dimmed to the lowest level. There was no behavioural task, but pauses were inserted about every 15 mins to ensure the vigilance of the subjects.

2.4. fNIRS recording and analysis

The fNIRS methodology used in the current study is largely the same as in Steinmetzger et al. (2022), where it is described in greater detail. fNIRS signals were recorded with a continuous-wave NIRScout 16x16 system (NIRx Medizintechnik, Berlin, Germany) at a sampling rate of 7.8125 Hz. Eight source optodes and eight detector optodes were placed symmetrically over each hemisphere by mounting them on an EEG cap with holes near the electrode sites P7 and P8 to accommodate the CI coils (EasyCap, Herrsching, Germany). The source optodes emitted infrared light with wavelengths of 760 and 850 nm. The chosen optode layout was devised to optimally cover the auditory cortex and associated areas. As the CI speech processors of most subjects hindered a stable scalp contact of optodes in the inferior temporal region, the corresponding channels (left: ch# 9 & 10; right: ch# 31 & 32) were excluded from the analyses. This resulted in 20 measurement channels per hemisphere, of which 18 had a standard source-to-detector distance of about 30 mm, while the remaining 2 had a shorter spacing of about 15 mm. The optode and reference positions for each individual subject were digitised with a Polhemus 3SPACE ISOTRAK II system (Colchester, VT, USA) before the recordings.

The raw data were pre-processed using the HOMER2 toolbox (version 2.8; Huppert et al. 2009) and custom MATLAB code. The raw light intensity signals were first converted to optical density values and then corrected for motion artefacts. A kurtosis-based wavelet algorithm with a threshold value of 3.3 was used to identify and correct motion artefacts (Chiarelli et al., 2015). Measurement channels with poor signal quality were then identified by computing their scalp coupling index (SCI; Pollonini et al. 2014) and excluded from further analysis if the SCI value was smaller than 0.6 (NH data sets: mean = 0.35 channels/subject, max 4 per subject; CI data sets: mean = 0.4, max = 3). Next, the motion-corrected signals of the remaining channels were band-pass filtered between 0.01 and 0.5 Hz to isolate the task-related neural activity, and subsequently converted to concentration values based on the modified Beer-Lambert law (Scholkmann et al., 2014). The differential path length factors required for the conversion were determined based on the wavelengths of the light and the age of the subject (Scholkmann and Wolf, 2013).

The pre-processed data were statistically evaluated and topographically visualised with SPM-fNIRS (version r3; Tak et al. 2016). The optode positions of each subject were first transformed from subject space to MNI space, after which they were probabilistically rendered onto the ICBM-152 cortical template surface (Singh et al., 2005). The signals were then temporally smoothed using the shape of the canonical haemodynamic response function (HRF, 'pre-colouring') to avoid auto-correlation issues (Worsley and Friston, 1995). The data of the individual subjects were statistically modelled by convolving the continuous signals obtained from each long channel with 16-s statistical parametric mapping (SPM) double-gamma functions representing the stimulus blocks. The oxygenated (HbO) and de-oxygenated (HbR) haemoglobin data were modelled with positive and negative HRFs, respectively. To allow the time course of the measured concentration changes to vary slightly, the temporal and spatial derivatives of the canonical HRF were included as additional regressors (Plichta et al., 2007). Furthermore, the signals from the four short channels were subjected to a principal component analysis, using the first component as an additional nuisance regressor to remove the so-called global scalp-haemodynamic component (Sato et al., 2016), i.e., the superficial signal component which is thought to not reflect cortical activity.

After estimating the HbO and HbR general linear models (GLMs) for each subject, contrast vectors were defined to assess the functional activations. When comparing the activity across ears or conditions, the regressors of interest were set to 1 and −1, respectively, while the regressors representing the derivatives and the global scalp component were set to 0 to statistically control for their effects. Likewise, when evaluating the activity within conditions, the respective regressors were set to 1, whereas all other regressors were set to 0. Group-level statistics of each contrast were then computed for each long channel by assessing the subject-level beta weights using one-sided *t*-tests.

A customised version of the SPM-fNIRS plotting routine was devised to visualise the optode and channel positions as well as the functional activations. The optode locations as well as the resulting channel positions and distances for the individual subjects are shown in Supplementary Fig. 1. Two auditory regions of interest (ROIs) were defined a priori, each comprising four channels positioned along the STC in both hemispheres (left ROI: ch# 5, 12, 14, and 16; right ROI: ch# 27, 34, 36, and 38). In the plots showing the functional activations, the short channels were omitted as they are assumed to not reflect any cortical responses. In the HRF plots, the subject-level waveforms were baseline corrected by subtracting the mean amplitude from −2–0 s around block onset from each sample point. The HRFs are shown both after the pre-processing ('Total HRF') as well as after regressing out the contribution of the short channels and pre-colouring the signals ('Cortical HRF'), to illustrate the effect of removing the non-cortical signal component. Additionally, the β-weighted canonical HRFs ('Modelled HRF') are shown to demonstrate how well the cortical HRFs can be explained by the GLM.

2.5. EEG recording and analysis

Continuous EEG signals were recorded using a 64-channel BrainVision actiCHamp system (Brain Products, Gilching, Germany). CI-compatible custom EEG caps with holes for the transmitter coils at electrode positions P7 and P8 were used. Apart from this deviation, the 60 scalp electrodes were arranged according to the extended international 10–20 system. Four additional electrodes were placed around the eyes to record vertical and horizontal eye movements. The EEG data were recorded with an initial sampling rate of 500 Hz, an online anti-aliasing low-pass filter with a cut-off frequency of 140 Hz, and were referenced to the right mastoid. The electrode positions of each subject were digitized with a Polhemus 3SPACE ISOTRAK II system before the experiment too.

The raw data were pre-processed offline using FieldTrip (version 20180924; Oostenveld et al. 2011) and custom MATLAB code. The continuous waveforms were first segmented into epochs ranging from −0.3–0.9 s relative to vowel onset. Next, linear trends and the DC component were removed by subtracting a 1st-order polynomial and the epochs were low-pass filtered at 15 Hz. The epochs were then re-referenced to the mean of both mastoids and down-sampled to 250 Hz. After visually identifying and excluding bad channels (NH data sets: mean = 1.25 channels/subject, max 7 per subject; CI data sets: mean = 1.8, max = 12), the data were decomposed into 20 principal components to detect and eliminate eye artefacts.

Pronounced CI artefacts were only evident in a subset of participants (8/20), for whom the principal component analysis was performed a second time to further reduce them (Schierholz et al., 2017; Schierholz et al., 2015). As CI artefacts are particularly large following sound on– and offset (Gilley et al., 2006; Viola et al., 2012), the use of continuous stimulus sequences appears to be the main reason for the relatively small artefact sizes in the current data (Pantev et al., 2006).

After the four eye electrodes were removed from the data, epochs in which the amplitudes between −0.2–0.8 s around stimulus onset exceeded ± 60 μV or the z-transformed amplitudes differed by more than 15 standard deviations from the mean of all channels were excluded from further processing. On average, 88% of the trials (1756/2000) passed the rejection procedure for the NH data sets and 87% for the CI data sets (1745/2000). In one subject, an unstable contact of the ground electrode led to data loss, so that only 42% (841/2000) of the NH trials and 36% (718/2000) of the CI trials remained after the rejection procedure. Lastly, bad channels were interpolated using the weighted average of the neighbouring channels, the data were re-referenced to the average of all 60 channels, and baseline corrected by subtracting the mean amplitude from −0.1–0 s before stimulus onset.

The pre-processed ERP data were then exported to BESA (version 5.2; BESA GmbH, Gräfeling, Germany; Scherg 1990) for source analysis. Based on the grand-average ERPs of the NH ears pooled across all trials, a source model with one current dipole per hemisphere was devised. A four-shell ellipsoidal head model was used. The time window used for fitting the model was centred around the P2 peak (216–372 ms). The dipole locations were constrained to be symmetrical across hemispheres, whereas the dipole orientations were estimated without constraints. For the grand-average ERPs obtained via the NH ears, this source model explained 94.96% of the variance in the data. To account for the lower signal-to-noise ratio of the data and to facilitate the comparability of the results between the ears, the same model was then applied without any alterations to the ERPs obtained via the CI ears too.

3. Results

3.1. fNIRS results

The group-level fNIRS HbR topographies are shown in Fig. 3A. The upper and middle rows depict the functional activations of each channel for the NH and CI ears compared to baseline level, whereas the lower row shows where the activity was stronger when the participants listened through the NH ears compared to the CI ears. The auditory cortex activity in these three contrasts was statistically evaluated by separately testing each channel included in the two auditory ROIs (left: ch# 5, 12, 14, & 16; right: ch# 27, 34, 36, & 38). The false discovery rate (FDR) across the ROI channels was controlled using the Benjamini-Hochberg procedure.

When the NH ears were stimulated, all eight ROI channels showed significant activity (averaged Cohen's d for right ROI = 1.08, left ROI = 0.74), whereas only two channels in the left ROI (ch# 5 & 16; average d = 0.55) reached significance level when the CI ears received auditory input (one-sample t-tests against 0, thresholded at $p_{(FDR)} < 0.05$). The comparison of both ears revealed significantly greater activity for three channels along the right STC (ch# 27, 34, & 36; right ROI: $d = 0.74$) and one channel near the left primary auditory cortex (ch# 12; left ROI: d = 0.44) for the NH ears (paired-samples t-tests, thresholded at $p_{(FDR)} <$ 0.05). Possible hemispheric lateralisation effects were then assessed by averaging the beta weights of the four channels in each ROI and comparing them across hemispheres. Paired t-tests indicated no hemispheric asymmetries for the NH ($t_{(19)} = 0.31$, $p = 0.759$) as well as the CI ears ($t_{(19)} = -0.54$, $p = 0.594$). To complement the topographical results, the corresponding HRFs are shown in Fig. 3B, separately for both ROIs. As for the topographies, the HRF amplitudes were markedly larger and more sustained for the NH ears.

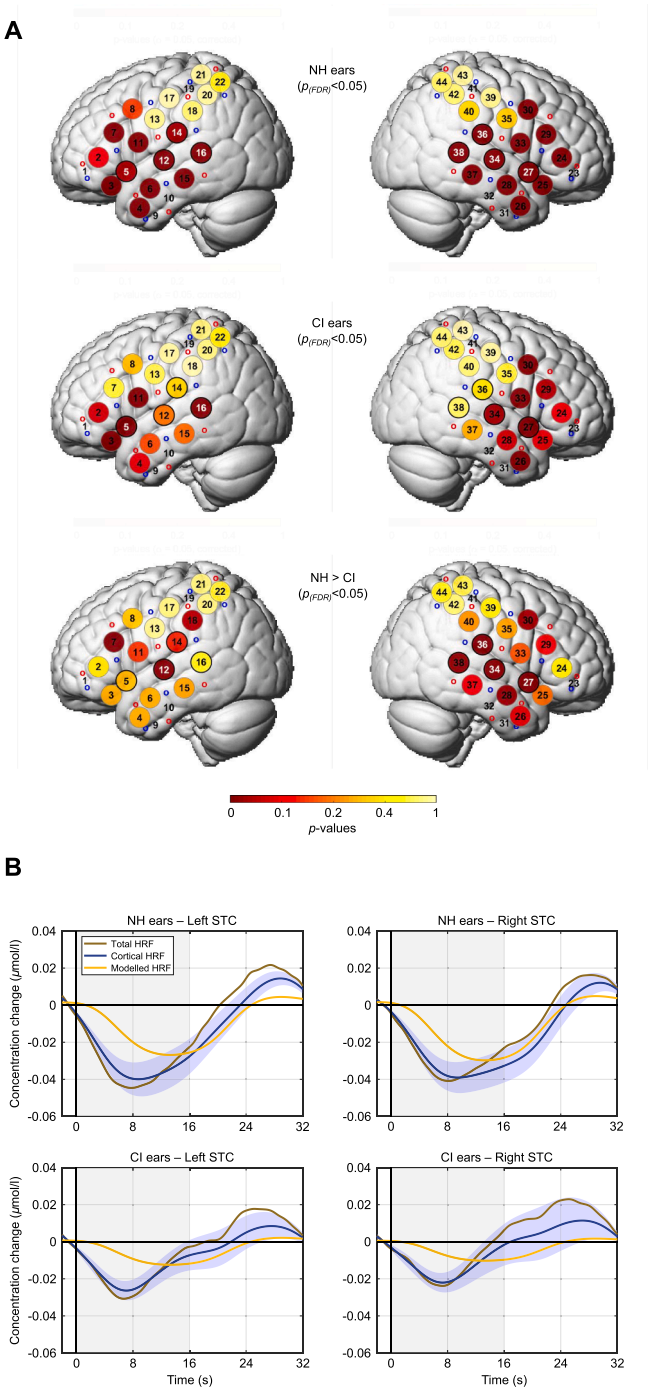

Fig. 3. fNIRS HbR results: comparison of the NH and CI ears. A) Topographies of cortical activity across conditions for both ears (upper two rows) as well as their statistical comparison (bottom row). Channels within the two auditory ROIs are outlined by black circles. White channel numbers indicate significant ROI channels. Significantly greater activity is evident for the NH ears, particularly in the right ROI. B) Group-level time courses for both ears and ROIs. The shading indicates the standard error of the mean.

We then compared the HbR topographies across the two stimulus conditions (Fig. 4, full results provided in Supplementary Fig. 2). For the NH ears, none of the channels in the two auditory ROIs showed greater activity in the VARIABLE PROSODY condition (paired-samples t-tests, thresholded at $p_{(FDR)} < 0.05$). Even when not correcting for multiple

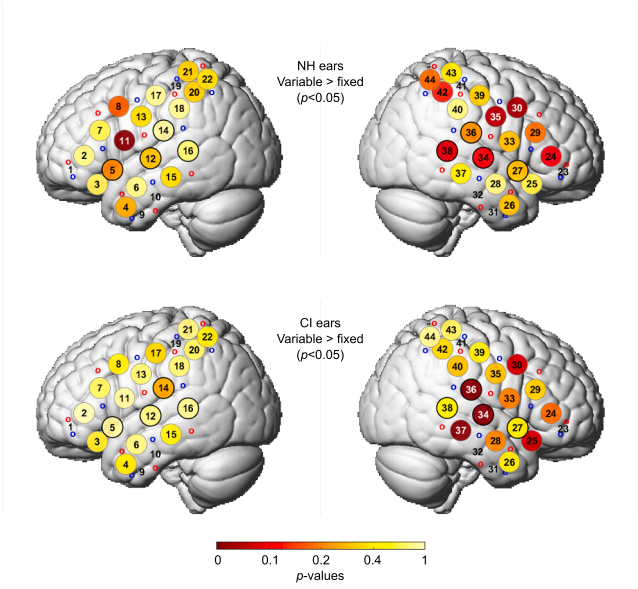

Fig. 4. fNIRS HbR results: comparison of the FIXED and VARIABLE PROSODY conditions. Topographies showing where the cortical activity in the VARIABLE PROSODY condition exceeded that in the FIXED PROSODY condition, separately for the NH and CI ears. White channel numbers indicate significance. Significant differences in auditory areas are only evident for the CI ears and in the right hemisphere.

comparisons, the trend in the posterior part of the right STC (ch# 38) did not reach significance level ($t_{(19)} = 1.64$, $p = 0.059$). For the CI ears, in contrast, two channels in the right ROI (ch# 34 & 36) as well as an adjacent channel (ch# 37) showed significantly greater activity in the VARIABLE PROSODY condition ($t \geq 2.39$, $p \leq 0.014$).

The corresponding fNIRS HbO results are provided in Supplementary Fig. 3. As in a previous auditory perception study with young NH listeners (Steinmetzger et al., 2020), the HbO topographies showed a prominent bilateral gradient with increasingly more negative effects in anterior-inferior direction. Rather than indicating a deactivation of fronto-temporal cortical areas, the fNIRS and EEG analyses in that paper demonstrated that this effect was associated with larger auditory ERPs and increased attention levels in the subjects who showed this pattern. Moreover, the negative HRFs observed here and in the earlier paper were found to lag behind the canonical HRF model considerably, suggesting that this effect does not reflect cortical activity but may be due to increased sympathetic nervous system activity (Kirilina et al., 2012; Tachtsidis and Scholkmann, 2016). However, as this gradient masks the underlying cortical activity in auditory cortex, we are focussing on the HbR data in the current paper.

3.2. EEG results

The sensor-level ERPs across all stimuli are shown in Fig. 5A, separately for both ears. The data show the pooled activity of a set of 16 electrodes in the fronto-central scalp region, where auditory ERPs typically have the largest amplitudes. The waveforms show a comparable morphology for both ears, with the characteristic transient ERP components (P1, N1, and P2) followed by a sustained potential (SP). A pronounced amplitude difference between the two ears is evident for the P2, which was markedly larger when the NH ears were stimulated. Permutation-based ($n = 10.000$) paired-samples *t*-tests for each time point during the stimulus window (0–800 ms) confirmed this observation, as differences between the two ears were confined to this period (212–276 ms, $p < 0.001$). Additionally, the N1 ($t_{(19)} = -4.59$, $p < 0.001$, $d = 1.03$; 176/198 ms) and the P2 ($t_{(19)} = -4.36$, $p < 0.001$, $d = 0.97$; 300/330 ms) peaked significantly earlier when the NH ears received auditory stimulation. The latency windows from which the respective peaks were extracted are based on the root-mean-square (RMS) waveforms of the grand-average ERPs across all channels. The scalp maps for each component time window and ear are shown on the right of Fig. 5A and exhibit similar distributions for both ears.

The corresponding source-level ERPs are shown in Fig. 5B. The cortical generators of the P2 were modelled using two dipoles located in the left and right planum temporale (MNI coordinates: ±43, −35, 13), posterior to primary auditory cortex. When averaging across both dipoles, the resulting source waveforms were very similar to the sensor-level ERPs described above: The largest amplitude differences were again observed for the P2 (208–296 ms, $p < 0.001$) and shorter latencies were evident for the N1 ($t_{(19)} = -5.79$, $p < 0.001$, $d = 1.29$; 171/196 ms), the P2 ($t_{(19)} = -3.30$, $p = 0.002$, $d = 0.74$; 292/330 ms), and also the SP ($t_{(19)} = -2.38$, $p = 0.014$, $d = 0.53$; 500/542 ms) when the NH ears were stimulated.

As shown in Fig. 5C, the dipole source modelling also allowed a separate analysis of the ERPs originating from both hemispheres. To aid the spatial comparison with the fNIRS results, the upper part of the figure shows the dipole locations after projecting them onto the surface of the template cortex used in the fNIRS analyses. The projected dipole positions corresponded to locations at the posterior end of the auditory fNIRS ROIs. The distance from the original positions to the scalp surface was about 41 mm (MNI coordinates: ±84, −35, 13).

The source waveforms revealed, firstly, that the P2 amplitude was significantly larger ($p < 0.001$) for the NH ears in both hemispheres. Additionally, the P2 emerging from the right hemisphere was found to have a longer latency for the NH ($t_{(19)} = 3.32$, $p = 0.004$, $d = 0.74$; 273/314 ms) as well as the CI ears ($t_{(19)} = 2.30$, $p = 0.033$, $d = 0.51$; 320/349 ms), but the comparison of the hemispheric differences across ears revealed no hemisphere*ear interaction ($t_{(19)} = 0.70$, $p = 0.495$). The dipole orientations also reflect this hemispheric difference, as the right dipole shows a distinctly more lateral orientation (Fig. 5B). Note that the apparent N1 amplitude difference across hemispheres is disregarded here as the dipole model was devised to localise the P2 rather than the N1, and the right dipole may thus only have captured parts of the N1.

Next, we examined whether the source-level ERP amplitudes were larger in the VARIABLE PROSODY condition than in the FIXED PROSODY condition (Fig. 5D). Surprisingly, no such effect was evident for the NH ears, neither for the P2 nor any other component. For the CI ears, in contrast, a significantly larger P2 amplitude (304–344 ms, $p < 0.05$) was observed in the right hemisphere. A similar pattern of results was also observed at the scalp level (Supplementary Fig. 4). Moreover, the source-level ERPs revealed an ear*condition interaction for a similar time window (316–336 ms, $p < 0.05$), reflecting that the condition difference for the P2 amplitudes was significantly larger for the CI ears.

3.3. Relation of fNIRS and EEG data with CI-based speech intelligibility

In a next step it was evaluated if the speech intelligibility scores that the participants achieved when listening through their CI ears (cf. Table 1) were reflected in the fNIRS and EEG data. When comparing the subjects with scores above and below the group median (55% words correct, $n = 8$ per subgroup), the fNIRS HbR data averaged across stimulus conditions indicated significantly greater activity in the posterior part of right auditory cortex (ch# 36; $t_{(14)} = 2.61$, $p = 0.01$, $d = 1.30$; independent-samples *t*-test) for the high intelligibility subgroup (Fig. 6A). Likewise, a significant negative correlation of the mean HbR amplitudes of all 20 subjects during the stimulus period (0–16 s) and their speech intelligibility scores was observed for channel 36 ($r_{(18)} = -0.54$, $p = 0.007$; Fig. 6A), while no other channel in the two auditory ROIs showed a similar effect ($p \geq 0.138$).

To further evaluate whether the gradient in the fNIRS HbO data reflects better auditory processing, the mean HbO amplitudes during the stimulus blocks (0–16 s) were then averaged across all channels in the two auditory ROIs and correlated with the CI speech intelligibility

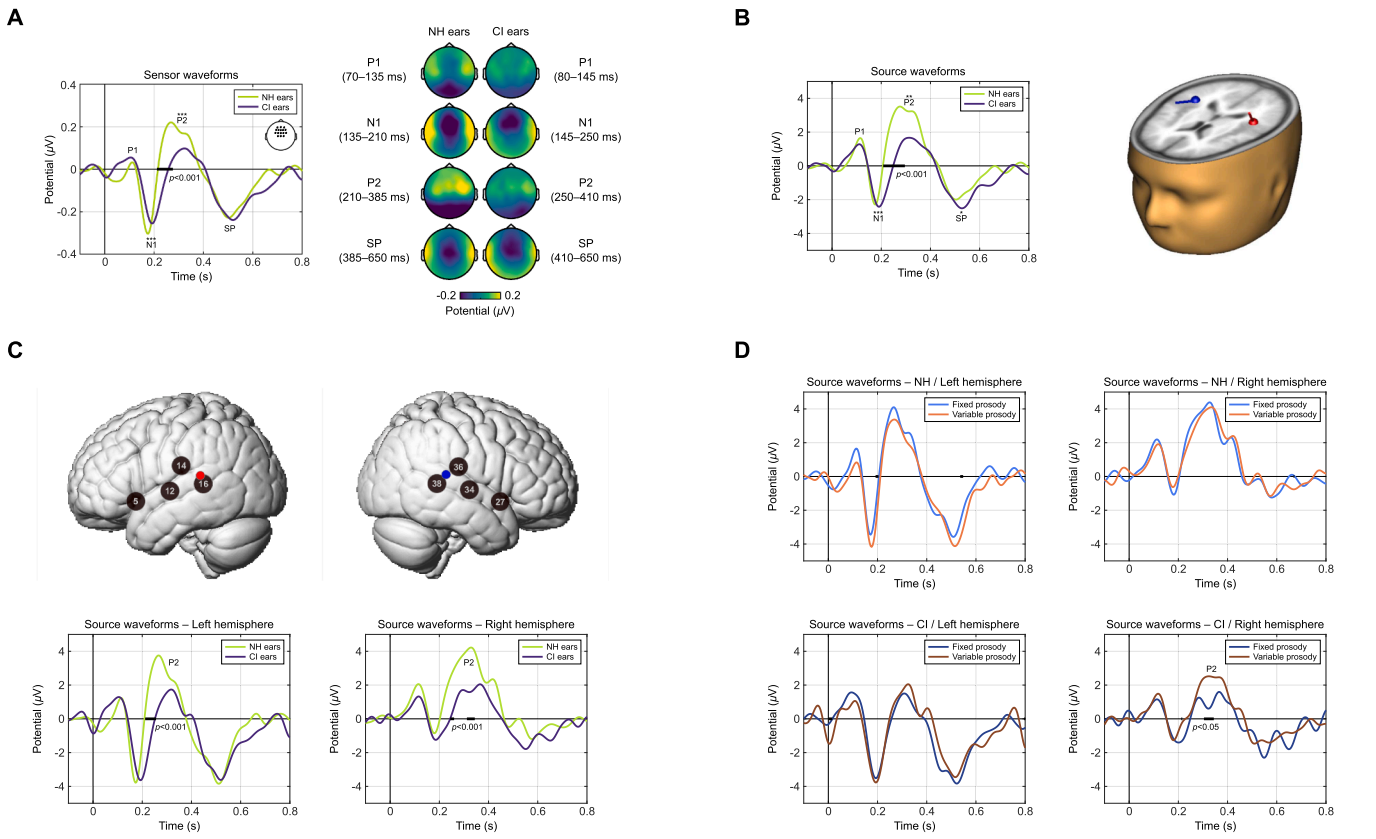

Fig. 5. EEG results. A) Sensor-level ERPs and scalp maps for the NH and CI ears, averaged across conditions. The ERPs were averaged over a set of electrodes in the fronto-central scalp region (see inset). The horizontal black bar in the ERP plot indicates a significant amplitude difference and the asterisks mark the significance level of the latency differences. B) Source-level ERPs and dipole locations. The ERPs were averaged across both dipoles. At both the sensor and source level, P2 amplitudes were larger and ERP latencies shorter for the NH ears. C) Source-level ERPs, separately for the left and right hemisphere. The upper row shows the fNIRS ROI channels along with the dipoles projected to the cortical surface. D) Source-level ERPs for the FIXED and VARIABLE PROSODY conditions, separately for both ears and hemispheres. Larger P2 amplitudes in the VARIABLE PROSODY condition were only observed for the CI ears and in the right hemisphere.

scores. As shown in Fig. 6B, the HbO amplitudes indeed exhibited a significant negative correlation with the percentage of correctly perceived words in the Freiburg monosyllabic speech test ($r_{(18)} = -0.48$, $p = 0.016$).

To complement the intelligibility effect observed in the fNIRS HbR data, it was furthermore tested whether the source-level ERPs of the dipole in the right hemisphere also reflect the CI-based speech intelligibility scores (Fig. 6C). For the right dipole, located near fNIRS channel 36, the transient ERPs in the high intelligibility subgroup were indeed more pronounced and significantly larger amplitudes were observed for the N1 ($p < 0.05$). Similarly, the subjects' N1 amplitudes (175–240 ms) in the right hemisphere and their intelligibility scores were negatively correlated ($r_{(18)} = -0.46$, $p = 0.02$).

4. Discussion

4.1. Smaller and delayed cortical responses in CI-based electric hearing

In the present study, auditory cortex activity evoked by acoustic and electric stimulation was directly compared in a group of unilateral adult CI users with SSD. A key finding is that cortical responses were larger when the NH ears received auditory stimulation, as evidenced by the fNIRS as well as the EEG data. The EEG results furthermore showed that the ERPs had significantly shorter latencies when the participants listened via their NH ears.

The fNIRS data revealed smaller responses for the CI ears, representing the first BOLD-based evidence of a difference between acoustic and electric hearing in the same group of participants. Specifically, the fNIRS HbR results indicated larger cortical activity along the right STC and near left primary auditory cortex for the NH ears. In contrast to a previous fNIRS-EEG study (Steinmetzger et al., 2022), in which young NH listeners tested with the same paradigm showed strongly right-lateralised activity, stimulation of both the NH and CI ears here led to relatively symmetric distributions of activity in auditory areas. For the CI ears, there was even a slight trend towards greater activity in the left hemisphere. With current CI systems, the access to spectral information is severely limited, whereas temporal envelope modulations are conveyed fairly accurately (Chatterjee and Peng, 2008; Macherey and Carlyon, 2014; Steinmetzger and Rosen, 2018). Models of auditory processing propose that the temporal resolution of the left auditory cortex is higher compared to the right one, which is in turn characterised by a greater spectral resolution (Poeppel, 2003; Zatorre et al., 2002). Accordingly, the trend for greater activity in the left hemisphere may reflect that the auditory input received via the CI ears contains more temporal than spectral information.

The corresponding ERP results showed that greater P2 amplitudes in response to stimulation of the NH ears seemed to underly the larger BOLD responses, suggesting that the P2 may be critically involved in the processing of voice pitch contours. Although the dipole source model of the P2 demonstrated that this effect was evident in both hemispheres,

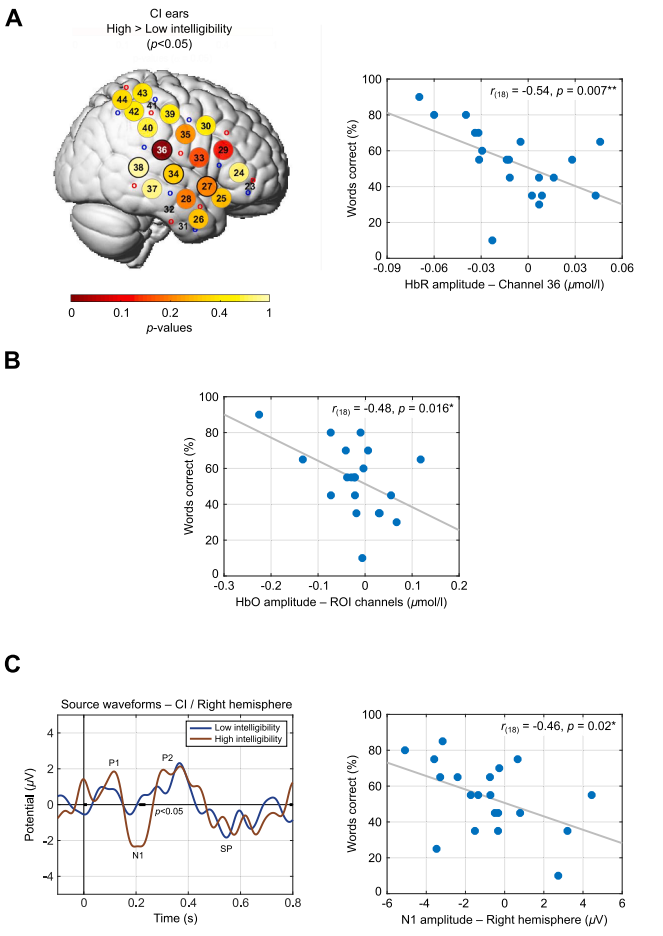

Fig. 6. CI-based speech intelligibility. A) fNIRS HbR topography of the contrast between subjects with high and low CI-based speech intelligibility scores. The latter subgroup showed significantly larger activity in the posterior part of the right auditory cortex (ch# 36). Furthermore, the HbR amplitudes at channel 36 and the intelligibility scores were negatively correlated. The words correct scores in the scatter plot are taken from Table 1. B) The fNIRS HbO amplitudes across all auditory ROI channels were also negatively correlated with speech intelligibility. C) The source-level ERPs of the dipole in the right hemisphere for both intelligibility subgroups. A larger N1 amplitude was evident in the high intelligibility subgroup and the right-hemispheric N1 amplitude was also negatively correlated with the speech intelligibility scores.

the P2 was found to peak later and have an extended duration in the right hemisphere. This hemispheric difference is also reflected in the more lateral orientation of the right dipole, which suggests that apart from primary auditory cortex the right STC was critically involved in generating the P2.

The side of implantation, on the other hand, did not appear to result in hemispheric asymmetries. Previous studies have reported that the N1 in response to monaural stimulation is larger in the contralateral hemisphere in acoustic (Hine and Debener, 2007; Hine et al., 2008) as well as electric hearing (Sandmann et al., 2009; Sandmann et al., 2015). However, no similar effect was observed for the P2 (Hine and Debener, 2007). Here, most subjects (13/20) wore their CI on the right and had preserved acoustic hearing in the left ear. As show in Supplementary Fig. 5, no asymmetries are evident in the fNIRS HbR topographies when considering participants with NH and CI ears on the right and left separately, and the same applies to the source-level ERPs which mainly reflected the unequal subgroup sizes.

Previous studies comparing ERPs in CI users and NH controls reported longer N1 and P2 latencies in electric hearing (Agrawal et al., 2013; Kelly et al., 2005; Sandmann et al., 2015; Viola et al., 2011; Wagner et al., 2017). The current results showed that this finding also applies to the subsequent sustained potential and, crucially, that delayed ERPs in CI-based electric hearing relative to acoustic hearing can also be observed within the same group of participants. Due to the small sample sizes, earlier SSD studies in which ERPs were obtained separately via both ears (Bönitz et al., 2018; Finke et al., 2016; Wedekind et al., 2021) have remained inconclusive regarding both latency and amplitude differences. These data thus show that even after several years of experience with their devices, the time course of cortical activity evoked by both types of hearing was still strikingly disparate. This is particularly noteworthy since none of the participants reported perceiving this discrepancy after an initial period of familiarisation with the CI.

Note that to avoid even longer testing times and because stimulating both ears separately allowed for easier interpretation of the data, we did not test the participants with their everyday bimodal setup. However, comparing combined acoustic and electric hearing to both types of hearing in isolation is certainly a worthwhile option for future studies.

4.2. *Saturation of cortical activity levels in acoustic hearing due to single-sided deafness*

A second major finding of the current experiment was that the auditory cortex activity elicited by the FIXED and VARIABLE PROSODY conditions did not differ significantly when the NH ears were stimulated, while the latter condition did evoke stronger responses when the CI ears were tested. For the NH ears, pronounced bilateral activity in auditory areas was evident in both conditions, but neither the fNIRS nor the EEG data indicated any difference between conditions or hemispheric lateralisation effects. In our previous fNIRS-EEG study with young NH listeners (Steinmetzger et al., 2022), on the other hand, increased activity along the right STC and larger ERPs in this region were observed in response to the VARIABLE PROSODY condition. Those results agreed with data showing that pitch changes are primarily processed in the anterior portion of the right STC in normal hearing (Johnsrude et al., 2000; Patterson et al., 2002; Zatorre et al., 2002).

The pronounced *F*0 changes of the prosodic contours and the audiograms of the NH ears, which in most cases only indicated some age-typical high-frequency hearing loss, rule out the possibility that the participants could not perceive the difference between both stimulus conditions when listening through their NH ears. Instead, the absence of a condition difference suggests a saturation of cortical activity levels. The pronounced but functionally unspecific auditory cortex responses observed here are likely a consequence of the preceding unilateral deafness period. In line with this explanation, studies with unilaterally deaf listeners have found a more symmetrical activation of auditory cortex compared to monaurally stimulated NH controls (Langers et al., 2005; Ponton et al., 2001). Moreover, the functioning ear has been shown to remain dominant in early-onset unilaterally deaf cats even after bilateral cochlear implantation (Kral et al., 2013).

4.3. *Differential processing of prosodic contours in electric hearing*

When testing the CI ears, the VARIABLE PROSODY condition was found to elicit stronger responses than the FIXED PROSODY condition. The fNIRS HbR data showed increased activity in the posterior part of the right STC, in agreement with the source-level ERPs which revealed that larger P2 amplitudes were generated in the posterior part of right auditory cortex. For the young NH listeners in our previous study (Steinmetzger et al., 2022), in contrast, the increase in activity in the VARIABLE PROSODY condition extended further anterior along the right STC and the ERP data indicated enhanced sustained potential amplitudes in addition to a larger P2. The results of both listener groups thus partially resemble each other and demonstrate that despite the limited access to pitch cues, prosodic variability results in right-lateralised processing in CI-based hearing too.

The tracking of pitch changes in normal hearing has been associated with right-lateralised activity in superior temporal regions anterior to primary auditory cortex (Johnsrude et al., 2000; Poeppel, 2003; Zatorre and Belin, 2001), even if the stimulus materials only contained temporal pitch cues (Patterson et al., 2002). Consequently, the lack of additional activity in those areas in the VARIABLE PROSODY condition suggests that even though the participants were able to differentiate between the two stimulus conditions, they relied on timbral cues rather than the pitch contours to do so (Oxenham, 2008). Nonetheless, this finding implies that the sensory input received via the implant contains enough information to supplement the contralateral normal ear, arguing in favour of fitting a CI to the deafened ear in unilateral deaf subjects.

Furthermore, the amount of activity in posterior right auditory areas coincided with speech intelligibility, as indicated by greater fNIRS HbR responses for channel 36 and increased N1 amplitudes for the right-hemisphere dipole. Thus, the same region that showed differential responses between the two stimulus conditions also reflected the participants' speech intelligibility scores. As spectral information is preferentially processed in right auditory areas, this finding may indicate a greater spectral resolution of the electric auditory input in subjects with high speech intelligibility.

5. Conclusions

The present study compared the cortical processing of voice pitch information in electric and acoustic hearing in a group of experienced unilateral CI users with contralaterally preserved acoustic hearing. Although poor transmission of pitch cues is a crucial factor underlying the difficulties CI user experience in noisy acoustic environments, it has remained unclear how the cortical processing of pitch information differs across both types of hearing.

The current fNIRS results showed that the pitch contours in natural vowels elicited bilateral activity in auditory cortex in electric as well as acoustic hearing, but that this activity was significantly smaller when the CI ears were stimulated. Coherent with the fNIRS data, the simultaneously obtained EEG data exhibited smaller and delayed ERPs in CI-based hearing. This pattern was particularly pronounced for the P2, which thus appears to reflect the processing of voice pitch information.

Additionally, both the fNIRS and EEG results showed that vowel sequences with variable rather than repeating pitch contours evoked additional activity in posterior right auditory cortex in electric but not acoustic hearing. This surprising finding demonstrates that the acoustic detail transmitted by CIs is sufficient to distinguish between speech sounds that only vary regarding their pitch information, while the functionally unspecific activity observed for the NH ears suggests a saturation of cortical activity levels.

Furthermore, when stimulating the CI ears, activity in this region was larger in subjects with higher CI-based speech intelligibility. This shows that the voice pitch-evoked cortical activity patterns obtained here are of diagnostic relevance, as they allow for a better understanding of the performance differences between CI users.

Funding

This work was supported by the Dietmar Hopp Stiftung (Grant No 2301 1239).

CRediT authorship contribution statement

Kurt Steinmetzger: Conceptualization, Methodology, Software, Formal analysis, Investigation, Writing – original draft, Writing – review & editing. **Bastian Meinhardt:** Investigation, Data curation, Project administration. **Mark Praetorius:** Conceptualization, Funding acquisition. **Martin Andermann:** Conceptualization, Funding acquisition, Writing – review & editing. **André Rupp:** Conceptualization, Funding acquisition, Supervision, Writing – review & editing.

Declaration of Competing Interest

The authors declare that they have no known competing financial interests or personal relationships that could have appeared to influence the work reported in this paper.

Data availability

The stimuli, fNIRS and EEG data, as well as the code used to process the data are all available at https://doi.org/10.17605/osf.io/9v6em.

Acknowledgements

We would like to thank Elisabeth Munk and Madhuri Sharma Rao for their help with recruiting the participants.

Appendix A. Supplementary data

Supplementary data to this article can be found online at https://doi.org/10.1016/j.nicl.2022.103188.

References

Agrawal, D., Thorne, J., Viola, F., Timm, L., Debener, S., Büchner, A., Dengler, R., Wittfoth, M., 2013. Electrophysiological responses to emotional prosody perception in cochlear implant users. NeuroImage: Clinical 2, 229–238. https://doi.org/10.1016/j.nicl.2013.01.001.

Anderson, C.A., Lazard, D.S., Hartley, D.E., 2017a. Plasticity in bilateral superior temporal cortex: effects of deafness and cochlear implantation on auditory and visual speech processing. Hearing Res. 343, 138–149. https://doi.org/10.1016/j.heares.2016.07.013.

Anderson, C.A., Wiggins, I.M., Kitterick, P.T., Hartley, D.E., 2017b. Adaptive benefit of cross-modal plasticity following cochlear implantation in deaf adults. Proc. Natl. Acad. Sci. USA 114, 10256–10261. https://doi.org/10.1073/pnas.1704785114.

Bisconti, S., Shulkin, M., Hu, X., Basura, G.J., Kileny, P.R., Kovelman, I., 2016. Functional near-infrared spectroscopy brain imaging investigation of phonological awareness and passage comprehension abilities in adult recipients of cochlear implants. J. Speech. Lang. Hear. Res. 59, 239–253. https://doi.org/10.1044/2015_JSLHR-L-14-0278.

Boemio, A., Fromm, S., Braun, A., Poeppel, D., 2005. Hierarchical and asymmetric temporal sensitivity in human auditory cortices. Nat. Neurosci. 8, 389–395. https://doi.org/10.1038/nn1409.

Bönitz, H., Kopp, B., Büchner, A., Lunner, T., Lyxell, B., Finke, M., 2018. Event-related neuronal responses to acoustic novelty in single-sided deaf cochlear implant users: Initial findings. Clin. Neurophysiol. 129, 133–142. https://doi.org/10.1016/j.clinph.2017.10.025.

Chatterjee, M., Peng, S.-C., 2008. Processing F0 with cochlear implants: Modulation frequency discrimination and speech intonation recognition. Hearing Res. 235, 143–156. https://doi.org/10.1016/j.heares.2007.11.004.

Chen, L.-C., Sandmann, P., Thorne, J.D., Bleichner, M.G., Debener, S., 2016. Cross-modal functional reorganization of visual and auditory cortex in adult cochlear implant users identified with fNIRS. Neural Plast. 2016, 4382656. https://doi.org/10.1155/2016/4382656.

Chen, L.-C., Puschmann, S., Debener, S., 2017a. Increased cross-modal functional connectivity in cochlear implant users. Sci. Rep. 7, 10043. https://doi.org/10.1038/s41598-017-10792-2.

Chen, L.-C., Stropahl, M., Schönwiesner, M., Debener, S., 2017b. Enhanced visual adaptation in cochlear implant users revealed by concurrent EEG-fNIRS. Neuroimage 146, 600–608. https://doi.org/10.1016/j.neuroimage.2016.09.033.

Chiarelli, A.M., Maclin, E.L., Fabiani, M., Gratton, G., 2015. A kurtosis-based wavelet algorithm for motion artifact correction of fNIRS data. Neuroimage 112, 128–137. https://doi.org/10.1016/j.neuroimage.2015.02.057.

Coez, A., Zilbovicius, M., Ferrary, E., Bouccara, D., Mosnier, I., Ambert-Dahan, E., Bizaguet, E., Syrota, A., Samson, Y., Sterkers, O., 2008. Cochlear implant benefits in deafness rehabilitation: PET study of temporal voice activations. J. Nucl. Med. 49, 60–67. https://doi.org/10.2967/jnumed.107.044545.

Everhardt, M.K., Sarampalis, A., Coler, M., Baskent, D., Lowie, W., 2020. Meta-analysis on the identification of linguistic and emotional prosody in cochlear implant users and vocoder simulations. Ear Hear. 41, 1092–1102. https://doi.org/10.1097/AUD.0000000000000863.

Finke, M., Sandmann, P., Bönitz, H., Kral, A., Büchner, A., 2016. Consequences of stimulus type on higher-order processing in single-sided deaf cochlear implant users. Audiology and Neurotology 21, 305–315. https://doi.org/10.1159/000452123.

Friesen, L.M., Picton, T.W., 2010. A method for removing cochlear implant artifact. Hearing Res. 259, 95–106. https://doi.org/10.1016/j.heares.2009.10.012.

Gilley, P.M., Sharma, A., Dorman, M., Finley, C.C., Panch, A.S., Martin, K., 2006. Minimization of cochlear implant stimulus artifact in cortical auditory evoked potentials. Clin. Neurophysiol. 117, 1772–1782. https://doi.org/10.1016/j.clinph.2006.04.018.

Giraud, A.-L., Truy, E., Frackowiak, R.S., Grégoire, M.-C., Pujol, J.-F., Collet, L., 2000. Differential recruitment of the speech processing system in healthy subjects and rehabilitated cochlear implant patients. Brain 123, 1391–1402. https://doi.org/10.1093/brain/123.7.1391.

Giraud, A.-L., Price, C.J., Graham, J.M., Frackowiak, R.S., 2001a. Functional plasticity of language-related brain areas after cochlear implantation. Brain 124, 1307–1316. https://doi.org/10.1093/brain/124.7.1307.

Giraud, A.-L., Price, C.J., Graham, J.M., Truy, E., Frackowiak, R.S., 2001b. Cross-modal plasticity underpins language recovery after cochlear implantation. Neuron 30, 657–664. https://doi.org/10.1016/S0896-6273(01)00318-X.

Green, T., Faulkner, A., Rosen, S., 2004. Enhancing temporal cues to voice pitch in continuous interleaved sampling cochlear implants. J. Acoust. Soc. Am. 116, 2298–2310. https://doi.org/10.1121/1.1785611.

Green, K.M., Julyan, P.J., Hastings, D.L., Ramsden, R.T., 2005. Auditory cortical activation and speech perception in cochlear implant users: effects of implant experience and duration of deafness. Hearing Res. 205, 184–192. https://doi.org/10.1016/j.heares.2005.03.016.

Hahlbrock, K.-H., 1953. Über Sprachaudiometrie und neue Wörterteste. Archiv f. Ohren-. Nasen- u. Kehlkopfheilkunde 162, 394–431. https://doi.org/10.1007/BF02105664.

Hine, J., Debener, S., 2007. Late auditory evoked potentials asymmetry revisited. Clin. Neurophysiol. 118, 1274–1285. https://doi.org/10.1016/j.clinph.2007.03.012.

Hine, J., Thornton, R., Davis, A., Debener, S., 2008. Does long-term unilateral deafness change auditory evoked potential asymmetries? Clin. Neurophysiol. 119, 576–586. https://doi.org/10.1016/j.clinph.2007.11.010.

Huppert, T.J., Diamond, S.G., Franceschini, M.A., Boas, D.A., 2009. HomER: a review of time-series analysis methods for near-infrared spectroscopy of the brain. Appl. Opt. 48, D280–D298. https://doi.org/10.1364/AO.48.00D280.

Johnsrude, I.S., Penhune, V.B., Zatorre, R.J., 2000. Functional specificity in the right human auditory cortex for perceiving pitch direction. Brain 123, 155–163. https://doi.org/10.1093/brain/123.1.155.

Kawahara, H., Irino, T., 2005. Underlying principles of a high-quality speech manipulation system STRAIGHT and its application to speech segregation. In: Divenyi, P. (Ed.), Speech Separation by Humans and Machines. Springer, Boston, MA, pp. 167–180.

Kelly, A.S., Purdy, S.C., Thorne, P.R., 2005. Electrophysiological and speech perception measures of auditory processing in experienced adult cochlear implant users. Clin. Neurophysiol. 116, 1235–1246. https://doi.org/10.1016/j.clinph.2005.02.011.

Kirilina, E., Jelzow, A., Heine, A., Niessing, M., Wabnitz, H., Brühl, R., Ittermann, B., Jacobs, A.M., Tachtsidis, I., 2012. The physiological origin of task-evoked systemic artefacts in functional near infrared spectroscopy. Neuroimage 61, 70–81. https://doi.org/10.1016/j.neuroimage.2012.02.074.

Kral, A., Hubka, P., Heid, S., Tillein, J., 2013. Single-sided deafness leads to unilateral aural preference within an early sensitive period. Brain 136, 180–193. https://doi.org/10.1093/brain/aws305.

Langers, D.R., van Dijk, P., Backes, W.H., 2005. Lateralization, connectivity and plasticity in the human central auditory system. Neuroimage 28, 490–499. https://doi.org/10.1016/j.neuroimage.2005.06.024.

Macherey, O., Carlyon, R.P., 2014. Cochlear implants. Curr. Biol. 24, R878–R884. https://doi.org/10.1016/j.cub.2014.06.053.

Mortensen, M.V., Mirz, F., Gjedde, A., 2006. Restored speech comprehension linked to activity in left inferior prefrontal and right temporal cortices in postlingual deafness. Neuroimage 31, 842–852. https://doi.org/10.1016/j.neuroimage.2005.12.020.

Mushtaq, F., Wiggins, I.M., Kitterick, P.T., Anderson, C.A., Hartley, D.E., 2020. The Benefit of Cross-Modal Reorganization on Speech Perception in Pediatric Cochlear Implant Recipients Revealed Using Functional Near-Infrared Spectroscopy. Front. Hum. Neurosci. 14, 308. https://doi.org/10.3389/fnhum.2020.00308.

Olds, C., Pollonini, L., Abaya, H., Larky, J., Loy, M., Bortfeld, H., Beauchamp, M.S., Oghalai, J.S., 2016. Cortical activation patterns correlate with speech understanding after cochlear implantation. Ear Hear. 37, e160–e172. https://doi.org/10.1097/AUD.0000000000000258.

Oostenveld, R., Fries, P., Maris, E., Schoffelen, J.-M., 2011. FieldTrip: open source software for advanced analysis of MEG, EEG, and invasive electrophysiological data. Comput. Intell. Neurosci. 2011, 1–9. https://doi.org/10.1155/2011/156869.

Oxenham, A.J., 2008. Pitch perception and auditory stream segregation: Implications for hearing loss and cochlear implants. Trends Amplif. 12, 316–331. https://doi.org/10.1177/1084713808325881.

Pantev, C., Dinnesen, A., Ross, B., Wollbrink, A., Knief, A., 2006. Dynamics of auditory plasticity after cochlear implantation: a longitudinal study. Cereb. Cortex 16, 31–36. https://doi.org/10.1093/cercor/bhi081.

Patterson, R.D., Uppenkamp, S., Johnsrude, I.S., Griffiths, T.D., 2002. The processing of temporal pitch and melody information in auditory cortex. Neuron 36, 767–776. https://doi.org/10.1016/S0896-6273(02)01060-7.

Pinti, P., Tachtsidis, I., Hamilton, A., Hirsch, J., Aichelburg, C., Gilbert, S., Burgess, P.W., 2018. The present and future use of functional near-infrared spectroscopy (fNIRS) for cognitive neuroscience. Ann. N. Y. Acad. Sci. 1464, 5–29. https://doi.org/10.1111/nyas.13948.

Plichta, M.M., Heinzel, S., Ehlis, A.-C., Pauli, P., Fallgatter, A.J., 2007. Model-based analysis of rapid event-related functional near-infrared spectroscopy (NIRS) data: a parametric validation study. Neuroimage 35, 625–634. https://doi.org/10.1016/j.neuroimage.2006.11.028.

Poeppel, D., 2003. The analysis of speech in different temporal integration windows: cerebral lateralization as 'asymmetric sampling in time'. Speech Commun. 41, 245–255. https://doi.org/10.1016/S0167-6393(02)00107-3.

Pollonini, L., Olds, C., Abaya, H., Bortfeld, H., Beauchamp, M.S., Oghalai, J.S., 2014. Auditory cortex activation to natural speech and simulated cochlear implant speech measured with functional near-infrared spectroscopy. Hearing Res. 309, 84–93. https://doi.org/10.1016/j.heares.2013.11.007.

Ponton, C.W., Vasama, J.-P., Tremblay, K., Khosla, D., Kwong, B., Don, M., 2001. Plasticity in the adult human central auditory system: evidence from late-onset profound unilateral deafness. Hearing Res. 154, 32–44. https://doi.org/10.1016/S0378-5955(01)00214-3.

Rouger, J., Lagleyre, S., Démonet, J.F., Fraysse, B., Deguine, O., Barone, P., 2012. Evolution of crossmodal reorganization of the voice area in cochlear-implanted deaf patients. Hum. Brain Mapp. 33, 1929–1940. https://doi.org/10.1002/hbm.21331.

Sandmann, P., Eichele, T., Buechler, M., Debener, S., Jäncke, L., Dillier, N., Hugdahl, K., Meyer, M., 2009. Evaluation of evoked potentials to dyadic tones after cochlear implantation. Brain 132, 1967–1979. https://doi.org/10.1093/brain/awp034.

Sandmann, P., Kegel, A., Eichele, T., Dillier, N., Lai, W., Bendixen, A., Debener, S., Jancke, L., Meyer, M., 2010. Neurophysiological evidence of impaired musical sound perception in cochlear-implant users. Clin. Neurophysiol. 121, 2070–2082. https://doi.org/10.1016/j.clinph.2010.04.032.

Sandmann, P., Plotz, K., Hauthal, N., de Vos, M., Schönfeld, R., Debener, S., 2015. Rapid bilateral improvement in auditory cortex activity in postlingually deafened adults following cochlear implantation. Clin. Neurophysiol. 126, 594–607. https://doi.org/10.1016/j.clinph.2014.06.029.

Sato, T., Nambu, I., Takeda, K., Aihara, T., Yamashita, O., Isogaya, Y., Inoue, Y., Otaka, Y., Wada, Y., Kawato, M., Sato, M.-A., Osu, R., 2016. Reduction of global interference of scalp-hemodynamics in functional near-infrared spectroscopy using short distance probes. Neuroimage 141, 120–132. https://doi.org/10.1016/j.neuroimage.2016.06.054.

Scherg, M., 1990. Fundamentals of dipole source potential analysis. Advances in audiology 6, 40–69.

Schierholz, I., Finke, M., Schulte, S., Hauthal, N., Kantzke, C., Rach, S., Büchner, A., Dengler, R., Sandmann, P., 2015. Enhanced audio–visual interactions in the auditory cortex of elderly cochlear-implant users. Hearing Res. 328, 133–147. https://doi.org/10.1016/j.heares.2015.08.009.

Schierholz, I., Finke, M., Kral, A., Büchner, A., Rach, S., Lenarz, T., Dengler, R., Sandmann, P., 2017. Auditory and audio–visual processing in patients with cochlear, auditory brainstem, and auditory midbrain implants: An EEG study. Hum. Brain Mapp. 38, 2206–2225. https://doi.org/10.1002/hbm.23515.

Scholkmann, F., Kleiser, S., Metz, A.J., Zimmermann, R., Pavia, J.M., Wolf, U., Wolf, M., 2014. A review on continuous wave functional near-infrared spectroscopy and imaging instrumentation and methodology. Neuroimage 85, 6–27. https://doi.org/10.1016/j.neuroimage.2013.05.004.

Scholkmann, F., Wolf, M., 2013. General equation for the differential pathlength factor of the frontal human head depending on wavelength and age. J. Biomed. Opt. 18 (10), 105004. https://doi.org/10.1117/1.JBO.18.10.105004.

Sevy, A.B., Bortfeld, H., Huppert, T.J., Beauchamp, M.S., Tonini, R.E., Oghalai, J.S., 2010. Neuroimaging with near-infrared spectroscopy demonstrates speech-evoked activity in the auditory cortex of deaf children following cochlear implantation. Hearing Res. 270, 39–47. https://doi.org/10.1016/j.heares.2010.09.010.

Singh, A.K., Okamoto, M., Dan, H., Jurcak, V., Dan, I., 2005. Spatial registration of multichannel multi-subject fNIRS data to MNI space without MRI. Neuroimage 27, 842–851. https://doi.org/10.1016/j.neuroimage.2005.05.019.

Steinmetzger, K., Megbel, E., Shen, Z., Andermann, M., Rupp, A., 2022. Cortical activity evoked by voice pitch changes: a combined fNIRS and EEG study. Hearing Res. 420, 108483 https://doi.org/10.1016/j.heares.2022.108483.

Steinmetzger, K., Rosen, S., 2018. The role of envelope periodicity in the perception of masked speech with simulated and real cochlear implants. J. Acoust. Soc. Am. 144, 885–896. https://doi.org/10.1121/1.5049584.

Steinmetzger, K., Shen, Z., Riedel, H., Rupp, A., 2020. Auditory cortex activity measured using functional near-infrared spectroscopy (fNIRS) appears to be susceptible to masking by cortical blood stealing. Hearing Res. 396, 108069 https://doi.org/10.1016/j.heares.2020.108069.

Strelnikov, K., Rouger, J., Demonet, J.-F., Lagleyre, S., Fraysse, B., Deguine, O., Barone, P., 2013. Visual activity predicts auditory recovery from deafness after adult cochlear implantation. Brain 136, 3682–3695. https://doi.org/10.1093/brain/awt274.

Strelnikov, K., Marx, M., Lagleyre, S., Fraysse, B., Deguine, O., Barone, P., 2015. PET-imaging of brain plasticity after cochlear implantation. Hearing Res. 322, 180–187. https://doi.org/10.1016/j.heares.2014.10.001.

Tachtsidis, I., Scholkmann, F., 2016. False positives and false negatives in functional near-infrared spectroscopy: issues, challenges, and the way forward. Neurophotonics 3 (3), 031405. https://doi.org/10.1117/1.NPh.3.3.031405.

Tak, S., Uga, M., Flandin, G., Dan, I., Penny, W., 2016. Sensor space group analysis for fNIRS data. J. Neurosci. Methods 264, 103–112. https://doi.org/10.1016/j.jneumeth.2016.03.003.

van de Rijt, L.P., van Opstal, A.J., Mylanus, E.A., Straatman, L.V., Hu, H.Y., Snik, A.F., van Wanrooij, M.M., 2016. Temporal cortex activation to audiovisual speech in normal-hearing and cochlear implant users measured with functional near-infrared spectroscopy. Front. Hum. Neurosci. 10, 48. https://doi.org/10.3389/fnhum.2016.00048.

Viola, F.C., Thorne, J.D., Bleeck, S., Eyles, J., Debener, S., 2011. Uncovering auditory evoked potentials from cochlear implant users with independent component analysis. Psychophysiology 48, 1470–1480. https://doi.org/10.1111/j.1469-8986.2011.01224.x.

Viola, F.C., De Vos, M., Hine, J., Sandmann, P., Bleeck, S., Eyles, J., Debener, S., 2012. Semi-automatic attenuation of cochlear implant artifacts for the evaluation of late auditory evoked potentials. Hearing Res. 284, 6–15. https://doi.org/10.1016/j.heares.2011.12.010.

Wagner, L., Plontke, S.K., Rahne, T., 2017. Perception of Iterated Rippled Noise Periodicity in Cochlear Implant Users. Audiology and Neurotology 22, 104–115. https://doi.org/10.1159/000478649.

Wedekind, A., Távora-Vieira, D., Nguyen, A.T., Marinovic, W., Rajan, G.P., 2021. Cochlear implants in single-sided deaf recipients: near normal higher-order processing. Clin. Neurophysiol. 132, 449–456. https://doi.org/10.1016/j.clinph.2020.11.038.

WHO, 2021. World report on hearing. https://www.who.int/publications/i/item/world-report-on-hearing.

Wilson, B.S., Dorman, M.F., 2008. Cochlear implants: a remarkable past and a brilliant future. Hearing Res. 242, 3–21. https://doi.org/10.1016/j.heares.2008.06.005.

Worsley, K.J., Friston, K.J., 1995. Analysis of fMRI time-series revisited—again. Neuroimage 2, 173–181. https://doi.org/10.1006/nimg.1995.1023.

Zatorre, R.J., Belin, P., 2001. Spectral and temporal processing in human auditory cortex. Cereb. Cortex 11, 946–953. https://doi.org/10.1093/cercor/11.10.946.

Zatorre, R.J., Belin, P., Penhune, V.B., 2002. Structure and function of auditory cortex: music and speech. Trends Cogn. Sci. 6, 37–46. https://doi.org/10.1016/S1364-6613(00)01816-7.

Zhou, X., Seghouane, A.-K., Shah, A., Innes-Brown, H., Cross, W., Litovsky, R., McKay C. M., 2018. Cortical speech processing in postlingually deaf adult cochlear implant users, as revealed by functional near-infrared spectroscopy. Trends in Hearing. 22, 2331216518786850. https://doi.org/10.1177/2331216518786850.